Int J Adv Manuf Technol (2011) 54:93–111
DOI 10.1007/s00170-010-2911-0

ORIGINAL ARTICLE

# Experimental and numerical analysis of titanium/aluminum clad metal sheets in sheet hydroforming

**Huang-Chi Tseng · Jung-Chung Hung · Chinghua Hung · Ming-Fu Lee**

Received: 13 May 2010 / Accepted: 22 August 2010 / Published online: 19 September 2010


**Abstract** Clad metals are becoming increasingly emphasized in sheet metal applications. In this research, sheet hydroforming process (SHF) was adopted to improve the formability of Ti/Al clad metal sheets and SUS 304 metal sheets used in computer, communication, and consumer product housings. Both finite element simulation and experimental verification were carried out to investigate the deformation of blanks. Several significant process parameters, such as holding force, friction, counter pressure history, and blank dimensions, were discussed for improving the formability of the two metal sheets. In SHF simulation, a virtual film technique was proposed to realistically approach the hydraulic loading condition during SHF. Finally, the deformed shape and thickness distribution of parts manufactured with SHF were compared with the results of simulation. Good agreements were obtained.

H.-C. Tseng · C. Hung
Department of Mechanical Engineering,
National Chiao Tung University,
Hsinchu 30050, Taiwan, Republic of China

J.-C. Hung
Department of Mechanical Engineering,
National Chin-Yi University of Technology,
Taiping City 411, Taiwan, Republic of China

M.-F. Lee
Metal Industries Research & Development Centre,
Kaohsiung, Taiwan, Republic of China

C. Hung (✉)
EE452, National Chiao Tung University,
1001 University Road,
Hsinchu, Taiwan 300, Republic of China
e-mail: chhung@mail.nctu.edu.tw

**Keywords** Clad metal · Sheet hydroforming · 3C product housing · FE simulation

## 1 Introduction

Electronics industries have been working to improve the surface quality of computer, communication, and consumer (3C) products using excellent metals such as titanium or stainless steel. However, since the formability of these metals is not as good as that of general metals (e.g., aluminum A1050), various material modifications and new forming techniques, including clad metal sheets and sheet hydroforming (SHF), have been developed to overcome this issue.

### 1.1 Clad metal

The clad metals considered in this study are multilayer sheets that possess various properties that surpass those of single metal sheets. Most clad metals not only preserve the original characteristics of the individual layer metals but also provide additional functional properties. In addition, some combinations of clad metal can effectively reduce the material cost in product applications.

Clad metal sheets are generally made from several processes, such as explosive bonding, adhesive bonding, hot roll bonding, and cold roll bonding. In this research, all clad metal sheets were made using cold roll bonding by MIRDC (Metal Industries Research & Development Center, Taiwan). In the cold roll bonding process, layer sheets are bonded together by interface diffusion while the thickness is reduced. The process has many advantages, such as accurate dimension control, fine surface quality, and straight bonding layers. The making of a two-ply clad metal sheet is illustrated

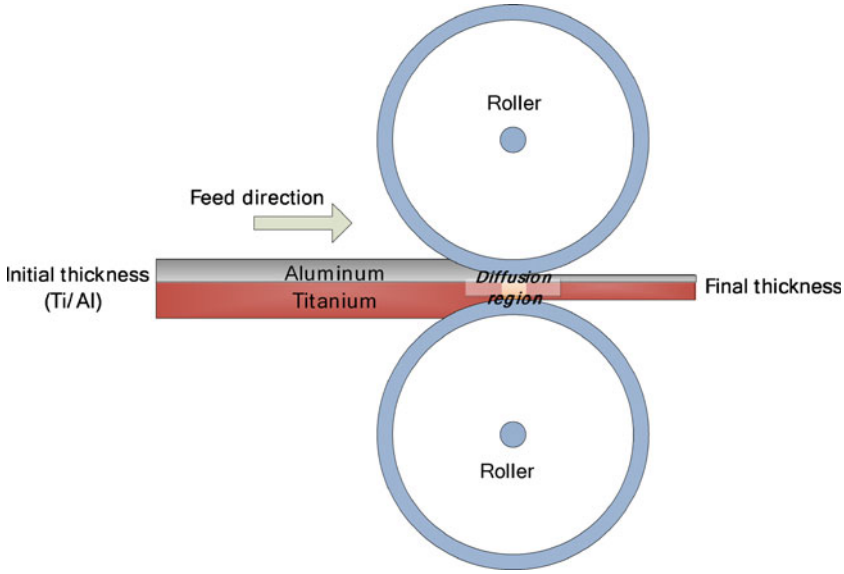


**Fig. 1** Schematic of the cold roll bonding of a two-ply clad metal sheet

in Fig. 1. The clad metal sheets are normally produced at room temperature, and the residual stresses generated in the rolling process cannot be fully released by the following annealing process because the melting temperatures of the individual layer sheets are often quite different. Therefore, the secondary formability of the clad metal sheets in the forming process must be considered and analyzed. Today, there have been some studies on the bonding performance of clad metal sheets with high diffusing temperature and long holding time [1–4], but there have been few studies done on the formability and application of clad metals produced at room temperature.

## 1.2 Sheet hydroforming

SHF is classified into SHF with a punch (SHF-P) and SHF with a die (SHF-D) depending on whether a punch or a die will be used to form the blank. Figure 2 shows a typical SHF-P process in which metal sheets are formed by a deep drawing punch with hydraulic counter pressure. The counter pressure is controlled by a relief valve, and an additional safety relief valve (not shown in Fig. 2) avoids bursting of the counter pressure pot. Nowadays, SHF is widely accepted for the industrial produced components characterized by fine surface quality, accurate dimensions, high drawing ratios, and complex shapes. Figure 3 shows SHF apparatus.

Today, there have been some studies on the formability of single material for different industries [5–9]. Some researchers proposed a multi-stage SHF which increased the formability of structural parts [10, 11]. A moveable inferior plate was adopted to enhance the SHF [12, 13]. Thiruvarudchelvan and Tan [14] provided a technique that uses a hydraulic pressure to apply a peripheral push on the flange, which applies a counter pressure in the die cavity that provides frictional support at the cup wall, and also provides excellent lubrication at the radius of the die. A modified hydromechanical deep drawing process was proposed and the experimental results compared with those obtained from the finite element method. Cylindrical cups made from aluminum with this process were drawn successfully with a drawing ratio as high as 3.0 [15].

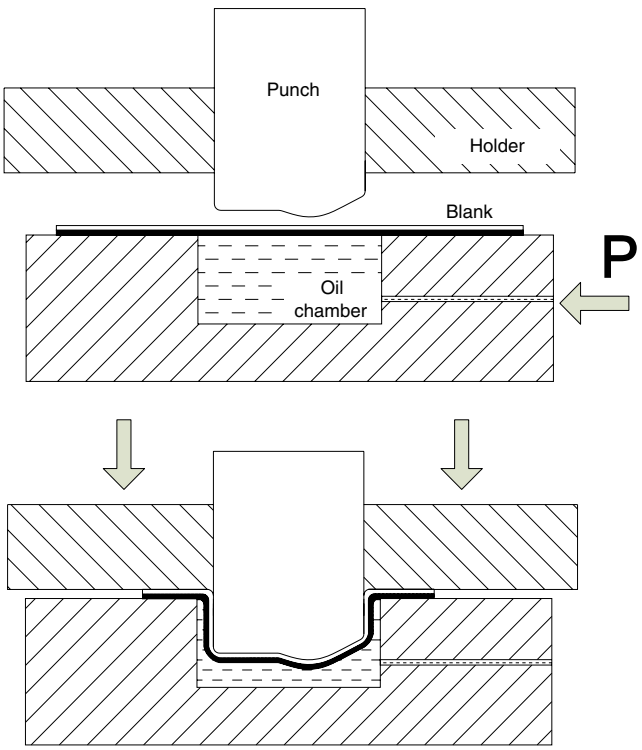


**Fig. 2** Schematic representation of SHF

**Fig. 3** SHF apparatus


For decades, finite element analysis (FEA) has become a well-established tool for predicting the formability of metal products and has enabled a significant reduction in the cost and time for design and also facilitated improvements in product quality. Kleiner et al. [16] investigated the residual stresses induced in high-fluid condition-formed workpieces by numerical and experimental analyses. The results showed that a higher fluid pressure leads to significantly lower residual stresses in addition to improved dimensional accuracy.

In general, most of the researches on SHF have analyzed the formability of a single material during the forming process; only few studies had been done on the formability of clad metal sheet product made by SHF. This research combines the advantages of both clad metal sheets and SHF

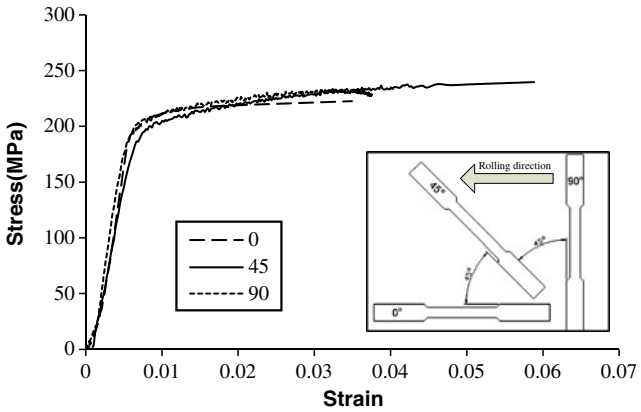


**Fig. 4** The true stress/strain curves of the Ti/Al clad metal sheets

**Table 1** Plastic strain ratios of Ti/Al clad metal

| $r_0$ | $r_{45}$ | $r_{90}$ |
|---|---|---|
| 0.913 | 2.591 | 0.941 |

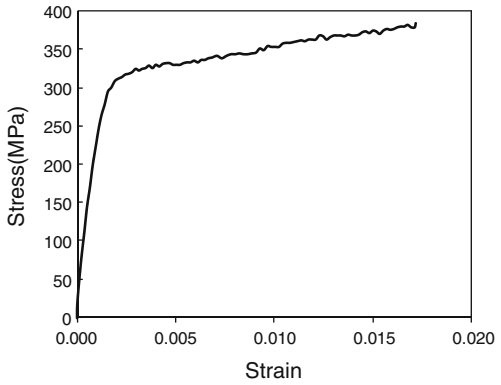


**Fig. 5** True stress/strain curves of the SUS 304 sheets

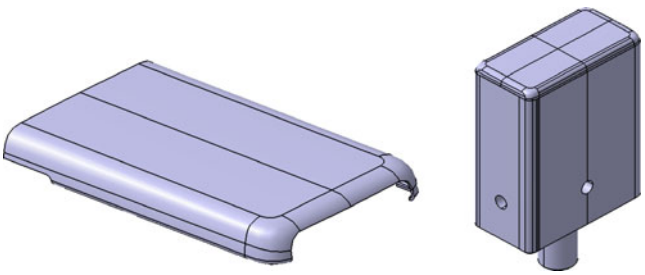

**Fig. 6** CAD model of housing I and punch

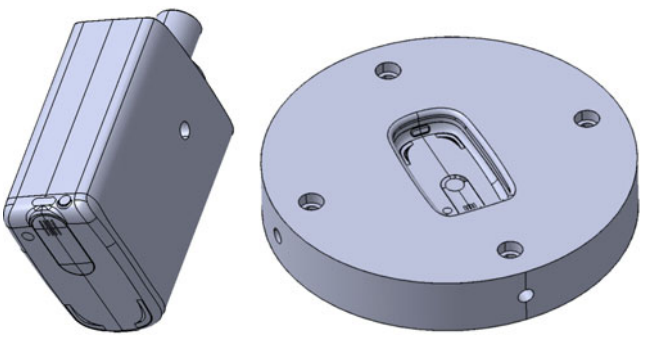

**Fig. 7** Die and punch for housing II

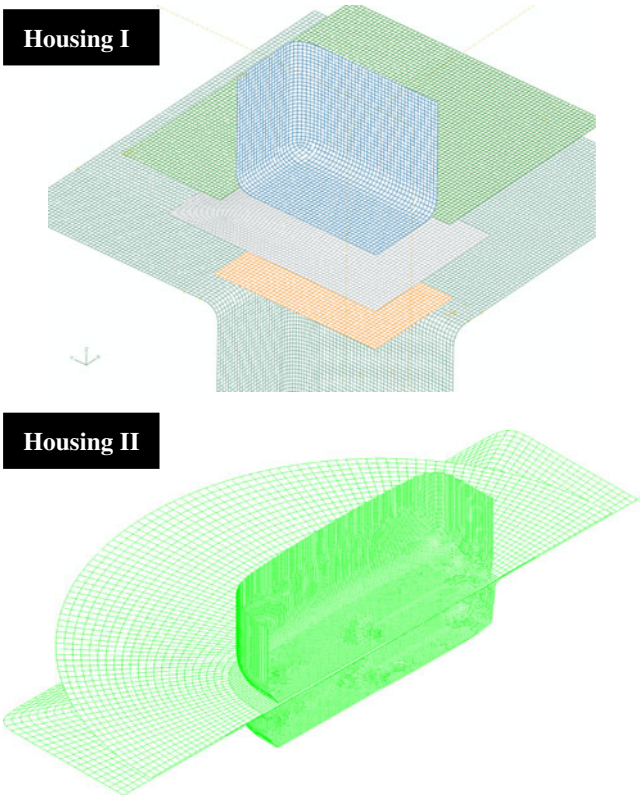


**Fig. 8** The FE meshes of housing I and housing II

in the application to 3C products. The reason for choosing Ti/Al clad metal sheets is that these clad sheets not only preserve the good surface quality of titanium but also reduce the cost of 3C housing products. Also, SHF is expected to improve the formability of Ti/Al clad metal sheets. In this research, several critical SHF process parameters were analyzed by FEA. For experimental verification, SUS 304 sheet was also deformed by SHF, and its formability was compared to that of the Ti/Al clad metal sheet by simulation and experiment.

## 2 Material property tests

Before material tests, all Ti/Al clad metal sheet specimens were prepared in the following manner. The individual layer materials were aluminum sheets 0.5 mm thick and titanium sheets 0.3 mm thick. The roll-bonded thickness of the clad metal sheet was 0.45 mm with a one-stage rolling process. For improving bonding strength and annealing residual stress, the clad metal sheet specimens were heated evenly to 500°C and then air-cooled for 1 h. Because the titanium part of the Ti/Al clad metal sheet was not fully annealed, the clad metal sheet was assumed to be anisotropic in FE simulations.

The plastic strain ratio, $r$, is considered a direct measure of sheet metal's drawability and is useful for evaluating materials intended for forming shapes by deep drawing. The $r$ value is the ratio of the true strain in the width direction to the true strain in the thickness direction when a sheet material is pulled in uniaxial tension beyond its elastic limit. The plastic strain ratio is calculated as shown in Eq. 1:

$$r = \frac{\varepsilon_w}{\varepsilon_t} \tag{1}$$

where $\varepsilon_w$ is the true width strain and $\varepsilon_t$ the true thickness strain.

To measure the mechanical properties of the Ti/Al clad metal sheets and SUS 304 sheets, tensile tests were carried out on a MTS-810 tensile machine. Figure 4 shows the true stress–strain curves obtained from Ti/Al clad metal sheets

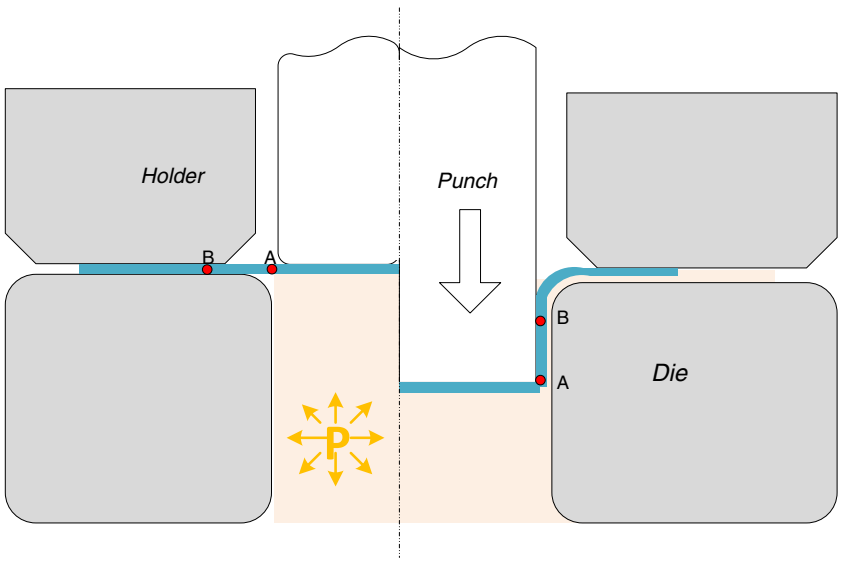


**Fig. 9** Schematic representation of various pressurized areas of the blank during SHF

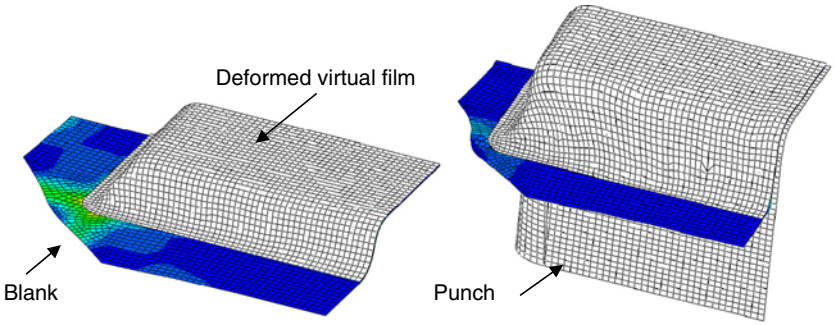


**Fig. 10** Operation of the virtual film with punch and blank

with three different directions (0°, 45°, and 90° with respect to rolling direction). Each curve represents the average result of three specimens. Table 1 shows the plastic strain ratio of Ti/Al clad metal. For comparison, SUS 304 sheets with a 0.45-mm thickness were also tensile tested. Figure 5 shows the true stress–strain curves of SUS 304. SUS 304 sheet was regarded as isotropic in FE simulations.

## 3 FE model

This section investigated SHF with Ti/Al clad metal sheets using ABAQUS. Two sets of 3C housings were analyzed. The CAD models are shown in Figs. 6 and 7. In housing I, a 1/4 symmetric model was utilized because of its symmetrical geometries. In housing II, a 1/2 symmetric model was utilized. During FE simulation, the interface condition of the clad metal sheet was assumed to be perfectly bonded and the Ti/Al clad metal sheet was regarded as an equivalent single material [17], with its material properties determined from previous tensile tests. The blank was meshed with quadrilateral shell elements, while the die, punch, and holder were simplified as discrete rigid bodies. The FE meshes for two housings are shown in Fig. 8.

In SHF simulations, the following assumptions and effects were applied for simplification and clarity:

- The clad metal is assumed to be an anisotropic, homogenous material.
- The bonding layer of the clad metal is perfect; the clad metal is assumed to be an equivalent single material.
- The deformation of the punch, holder, and die was neglected.
- Leakage of fluid was neglected.
- The interface coefficient of friction was assumed to be constant.

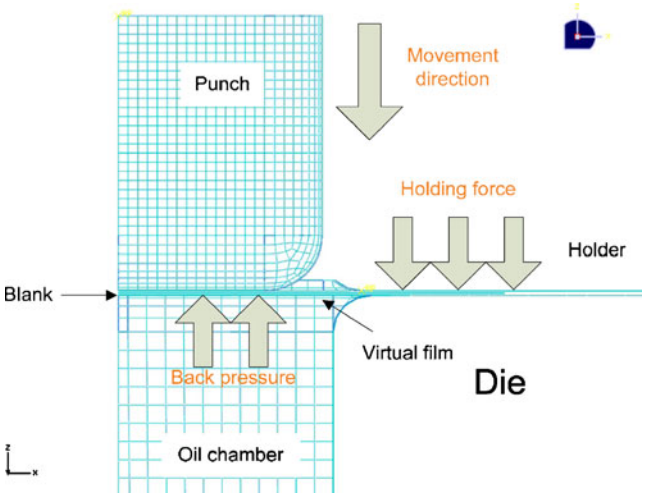


**Fig. 11** Boundary condition of the FE model

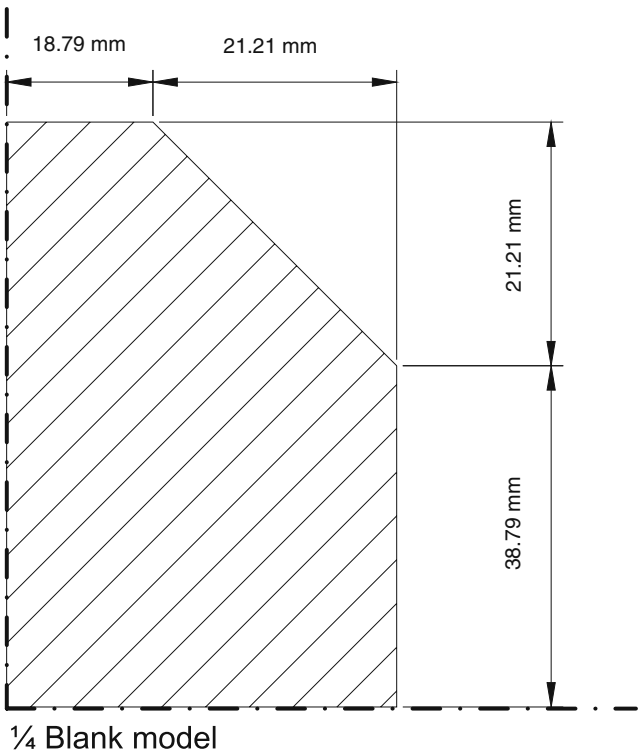


**Fig. 12** Blank dimensions for housing I

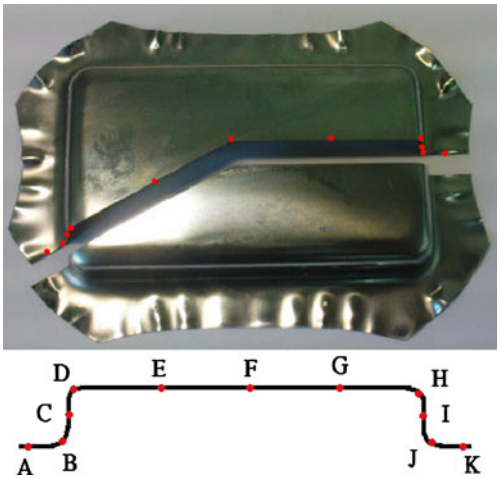


**Fig. 13** Locations of measured points on housing I

For boundary conditions, three contact pairs (punch–blank, holder–blank, and blank–die) were defined in this FE model. The Coulomb coefficient of friction was set to 0.05 and 0.1 for contact surfaces with and without lubrication [10, 18].

The punch was specified to move only in the *z* direction, and a holding force was applied to the blank through the holder. In SHF, the pressurized area of the blank was varied according to movements of the punch, as shown in Fig. 9. Therefore, a concept of applying a virtual film was proposed to realistically simulate the hydraulic loading of the blank during SHF simulation. In FE model, authors create a thin shell element (the thickness is 0.01 mm) between the blank and die cavity. The Young's module of the thin shell element is smaller than the clad metal. The coefficient of friction for the contact pair of blank–virtual film was set to zero. During SHF, the hydraulic loading can realistically translate to blank by a contact behavior of both parts. Figure 10 shows the operation of the virtual film with the die and punch. Figure 11 summarizes the boundary conditions of the SHF FE model.

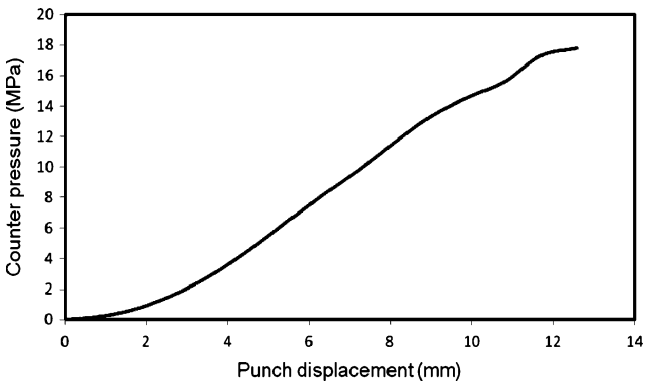


**Fig. 14** Measured counter pressure history

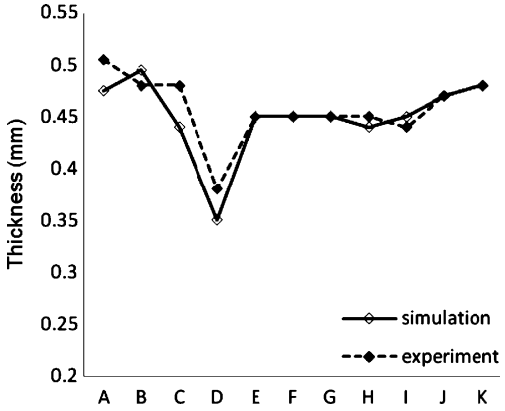


**Fig. 15** Comparison of thickness distributions of the experiment with the simulation

## 4 Analysis of the application of SHF on housing I

### 4.1 FE model verification

In this section, the model of housing I was analyzed. First, the FE model was verified by comparing the thickness distribution of product from experiment. Figure 12 shows the blank dimension (1/4 symmetry), and Fig. 13 shows the locations of the measured points on sheet. The preliminary experiment parameters were a punch displacement of 13.5 mm, a holding force of 2 t, and the counter pressure history was according to the measured values with a pressure gauge, as shown in Fig. 14.

Figure 15 shows the good agreement of thickness distribution between the experiment and the simulation. In the next sections, some critical process parameters will be analyzed by this validated FE model and a term called the

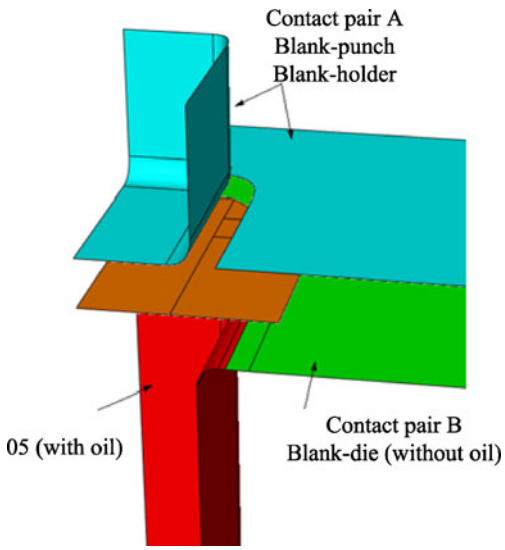


**Fig. 16** Schematic representation of different contact pairs in SHF

**Table 2** Combinations of coefficients of friction for contact pairs A and B

| | Contact pair A | Contact pair B |
|---|---|---|
| Condition 1 | 0.1 | 0.05, 0.1, 0.2 |
| Condition 2 | 0.05, 0.1, 0.2 | 0.1 |

thinning ratio distribution of the blank will be used. The thinning ratio is defined as:

$$\text{Thinning ratio} = \frac{T_0 - T_1}{T_0} \times 100\% \quad (2)$$

where $T_1$ is the final blank thickness and $T_0$ is the initial blank thickness.

## 4.2 Influence of the coefficient of friction

During SHF, the friction condition differed with and without lubricant, and the contact materials of the clad metal were also different for the holder and die (outside of the seal); therefore, the influence of the coefficient of friction is crucial.

In this research, various combinations of friction conditions were assigned in simulation. Figure 16 shows the setting of different contact pairs in SHF, and Table 2 shows the combinations of $\mu$ for different contact pairs. The coefficient of friction $\mu$ was set to 0.05 in an oil chamber. Other process parameters were a punch displacement of 13.5 mm, holding force of 2 t, and a maximum counter pressure of 10 MPa. The increase of counter pressure was assumed to be linear during FE simulation.

Figure 17 shows the thinning ratio distributions of the blank under condition 1. Thinning of the blank occurs at points C, D, and I when the coefficient of friction of the blank–die contact pair increases. However, these thinning results are close because the friction effect between the blank and the die (contact pair B) is small.

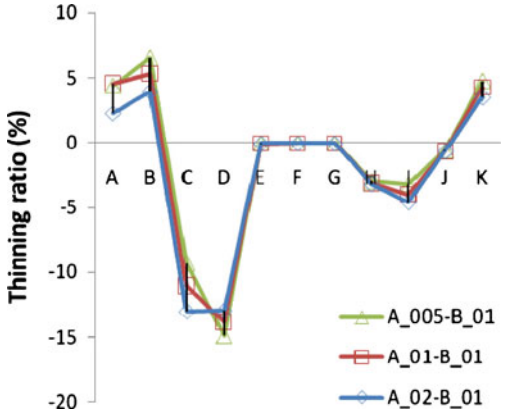


**Fig. 18** Thinning ratio distribution under condition 2 (contact pair B=0.1)

As shown in Fig. 18, points C and D have opposite thinning trends compared to the other points when the coefficients of friction of contact pair A (blank–punch) are increased. Compared to the results at point D, a higher coefficient of friction condition ($\mu$=0.2) with the counter pressure effect has been helpful for drawing. In addition, for SHF, sufficient friction force between punch and blank has been helpful for drawing.

## 4.3 Influence of the holding force

In general deep drawing process, the holding force is a positive parameter for product formability, but a large holding force might create too much restraining force for metal flow. For SHF, an insufficient holding force causes wrinkling and creates additional leakage problems. In this section, the effects of different holding forces were simulated. The Coulomb coefficient of friction was set to 0.05 (blank–die) and 0.1 (punch–blank and holder–blank)

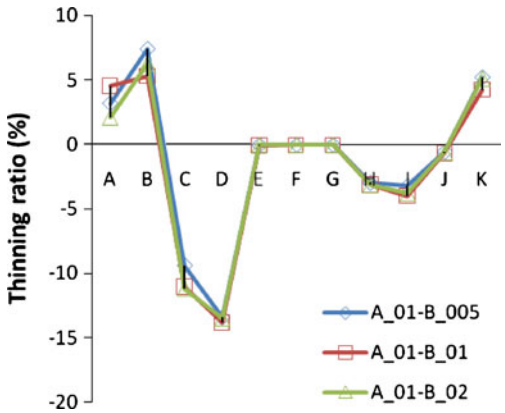


**Fig. 17** Thinning ratio distributions under condition 1 (contact pair A=0.1)

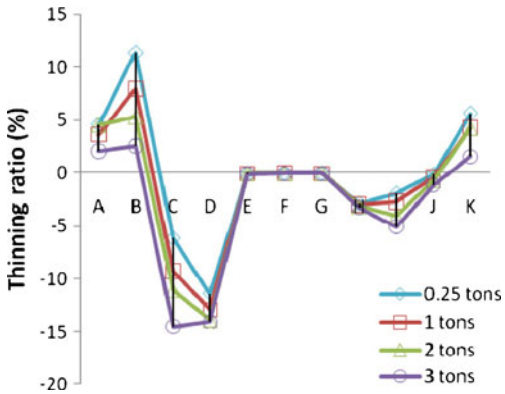


**Fig. 19** Thinning ratio distribution of the blank with different holding forces

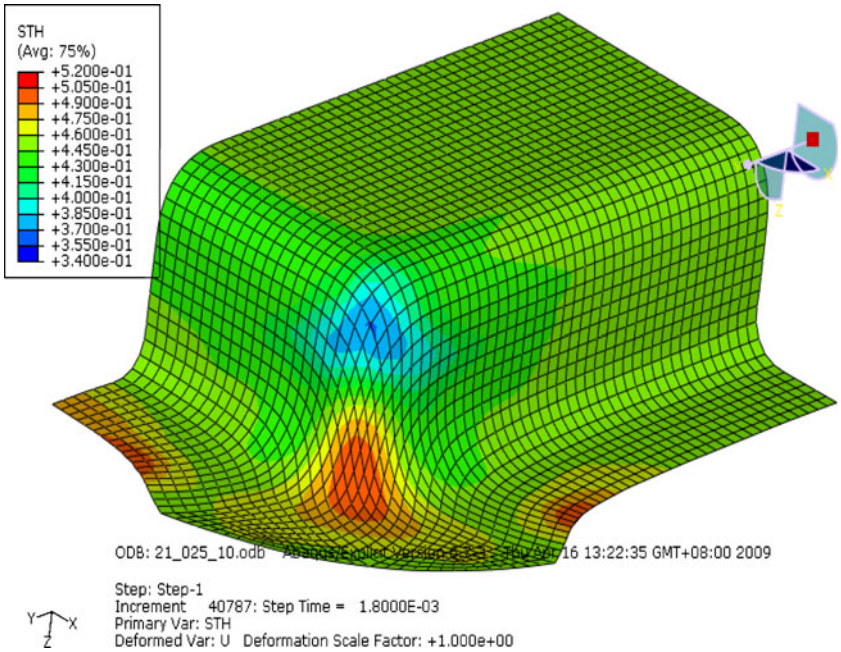


**Fig. 20** The thickness distribution of the blank without wrinkling (holding force=0.25 t)

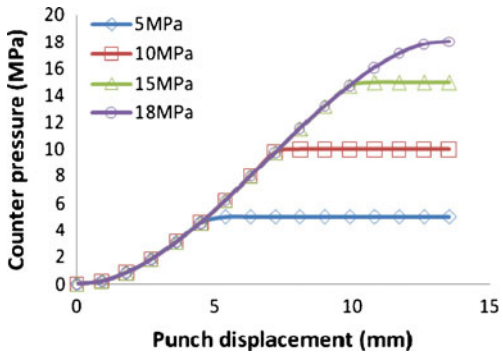


**Fig. 21** Different counter pressure histories

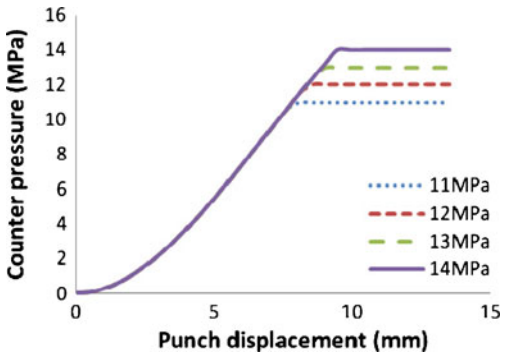


**Fig. 23** Different counter pressure histories (final pressure 11–14 MPa)

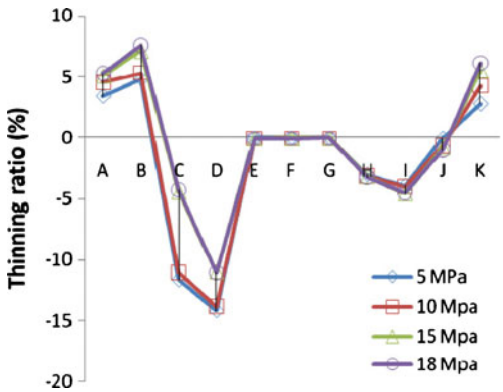


**Fig. 22** Thinning ratio distributions with different counter pressure histories

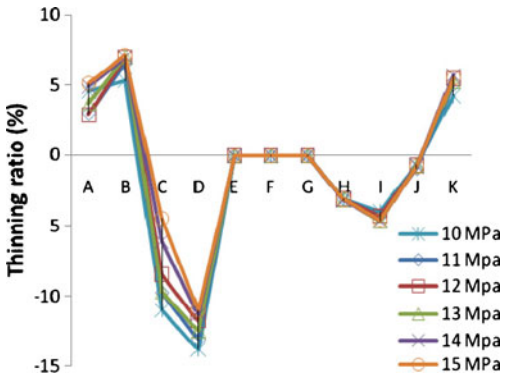


**Fig. 24** Thinning ratio distributions with different counter pressure histories (final pressure 10–15 MPa)

**Table 3** Combinations of process parameters for housing II

| Material | SUS 304 | | | Ti/Al | |
|---|---|---|---|---|---|
| Holding force (tons) | 0.7 | 1 | 2 | 0.7 | 1 |
| Chamfer width (blank dimension) | 20 (114×74) | 21.21 (120×80) | 20 (114×74), 21.21(120×80), 23 (120×80) | 20 (114×74) | |

Length unit: mm. Measured counter pressure histories were used for each case in simulation. Blank dimension (length×width)

for contact surfaces with and without lubrication. Other process parameters are a punch displacement of 13.5 mm, a maximum counter pressure of 10 MPa, and the counter pressure history was assumed to be linear during FE simulation. Figure 19 shows the thinning ratio distributions with different holding forces.

Simulations show that the thinning trend of the blank was affected by the holding force. Because there was no wrinkling of the blank, a small holding force (0.25 t) was favored in this application, as shown in Fig. 20.

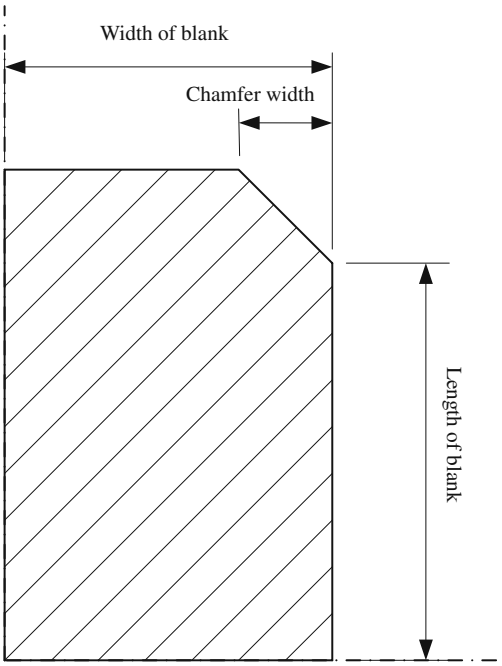


**Fig. 26** Representation of the blank dimension

## 4.4 Influence of counter pressure history

Compared to a conventional stamping process, SHF can provide counter pressure to a blank, which can hold the blank closer to the punch. Oil lubrication is also helpful in reducing the friction between the die and blank.

In this section, different counter pressure histories were analyzed to see how they improved the formability of the clad metal. Figure 21 shows the different counter pressure histories used in the analysis. The Coulomb coefficient of friction was set to 0.05 (blank–die) and 0.1 (punch–blank and holder–blank) for contact surfaces with and without lubrication. Other process parameters were a punch displacement of 13.5 mm and a holding force of 2 t. Figure 22 shows the simulation results.

These results show that the thinning ratio of the blank was reduced by an increase in counter pressure. Compared to the cases of 5 MPa with 10 MPa and 15 MPa with 18 MPa, it shows that the thinning ratio distributions were close to each other at high pressure cases. Four additional different pressure histories (final counter pressures are 11, 12, 13, and 14 MPa, shown in Fig. 23) were simulated again to verify the effect of counter pressure. Figure 24 shows the thinning ratio distribution of a blank with different pressure histories. A large final pressure (in this case 15 MPa) improves the formability of the blank most.

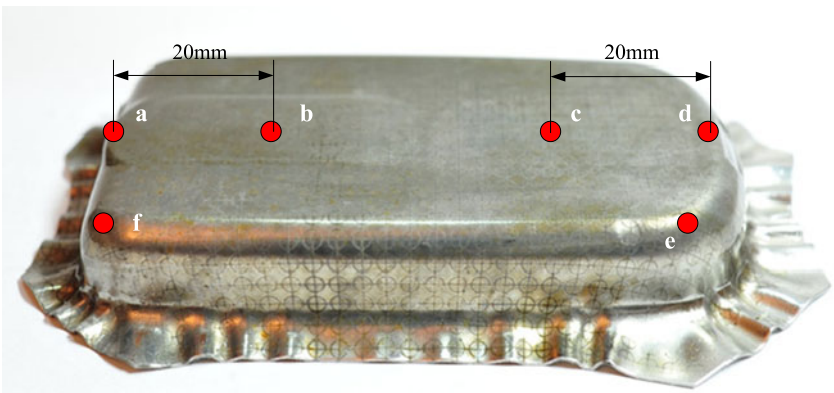


**Fig. 25** Locations of measured points on housing II

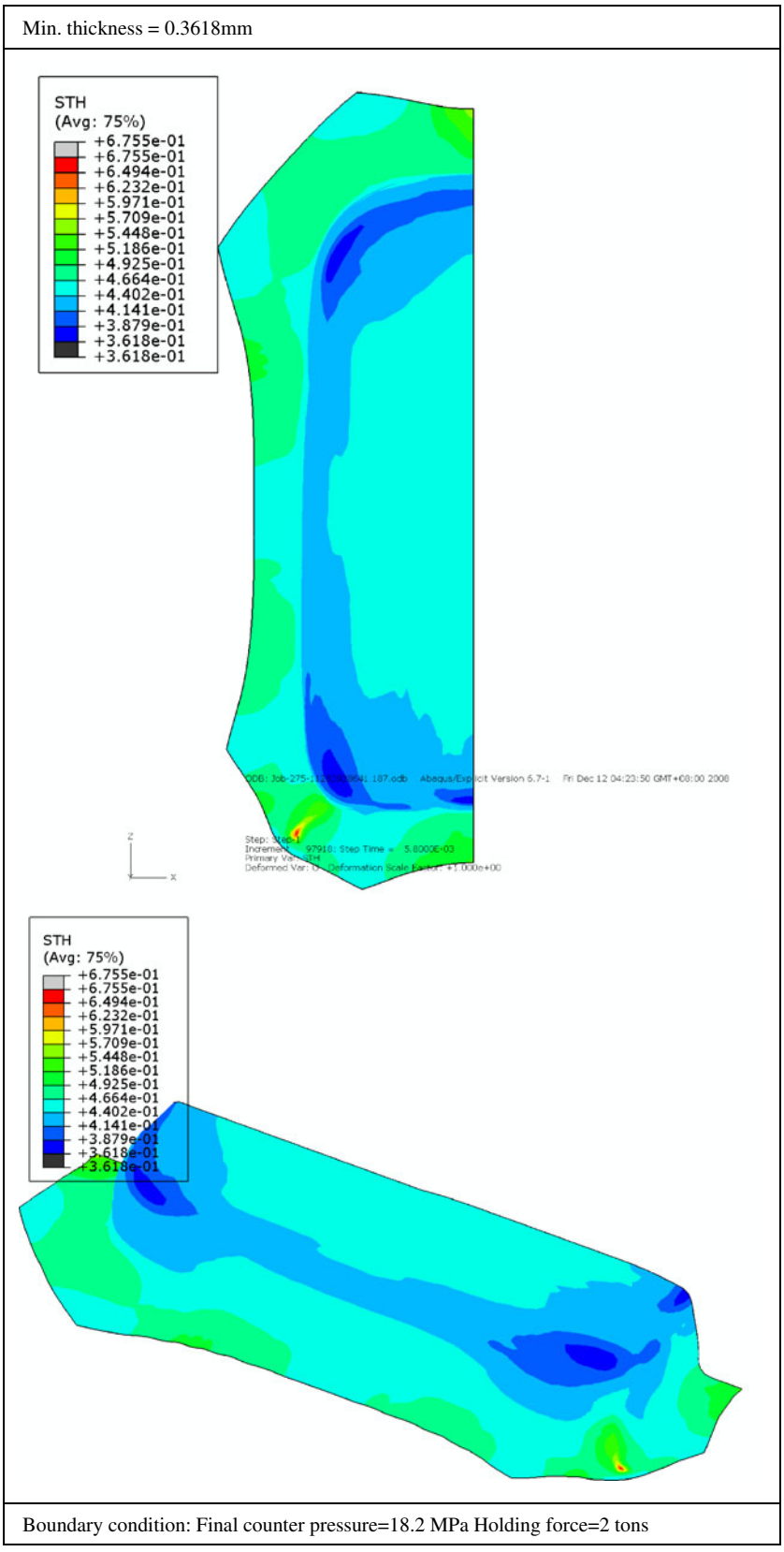


**Fig. 27** The thickness distribution of the blank (chamfer width=21.21 mm, SUS 304)

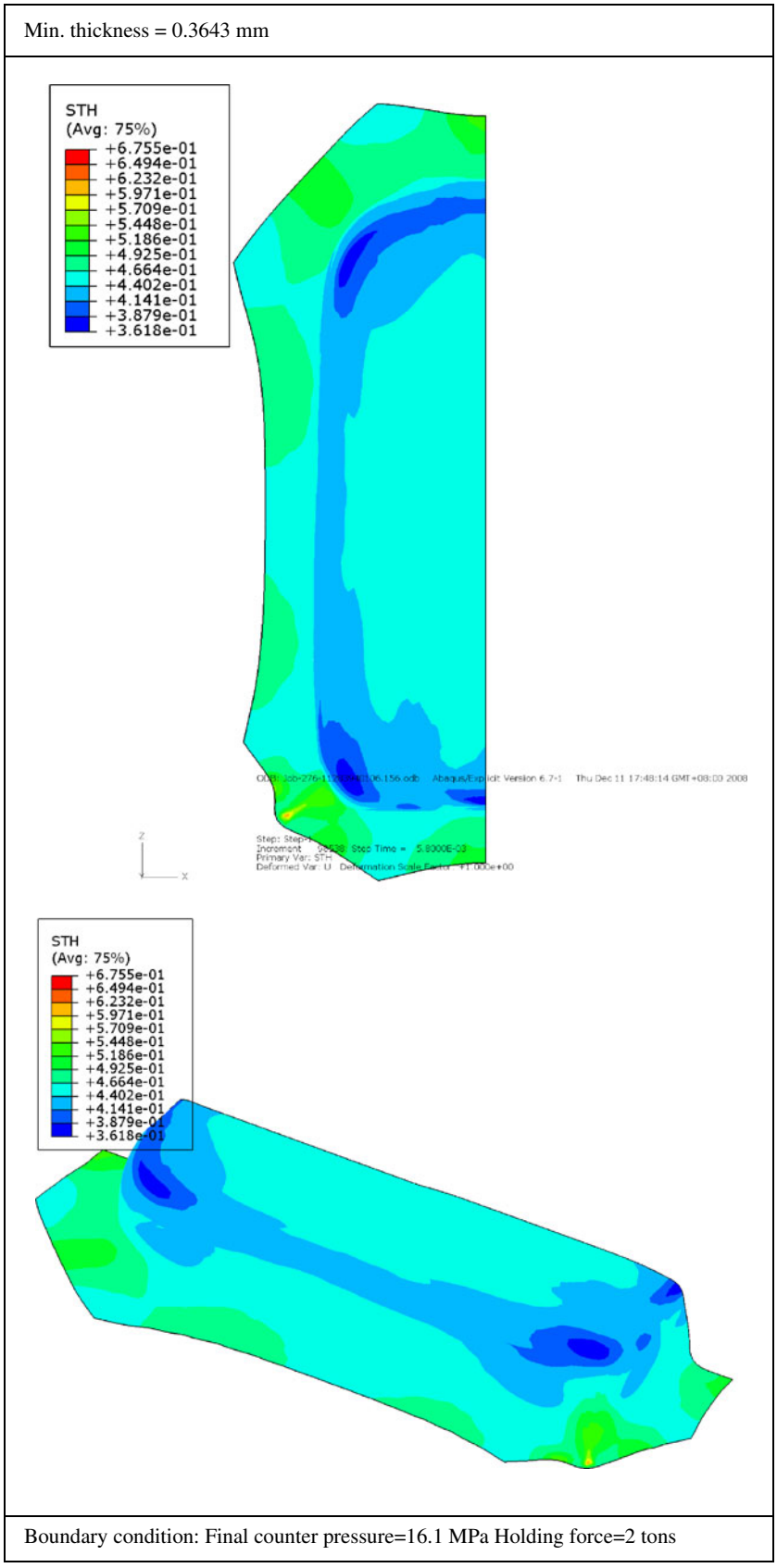


**Fig. 28** The thickness distribution of the blank (chamfer width=23 mm, SUS 304)

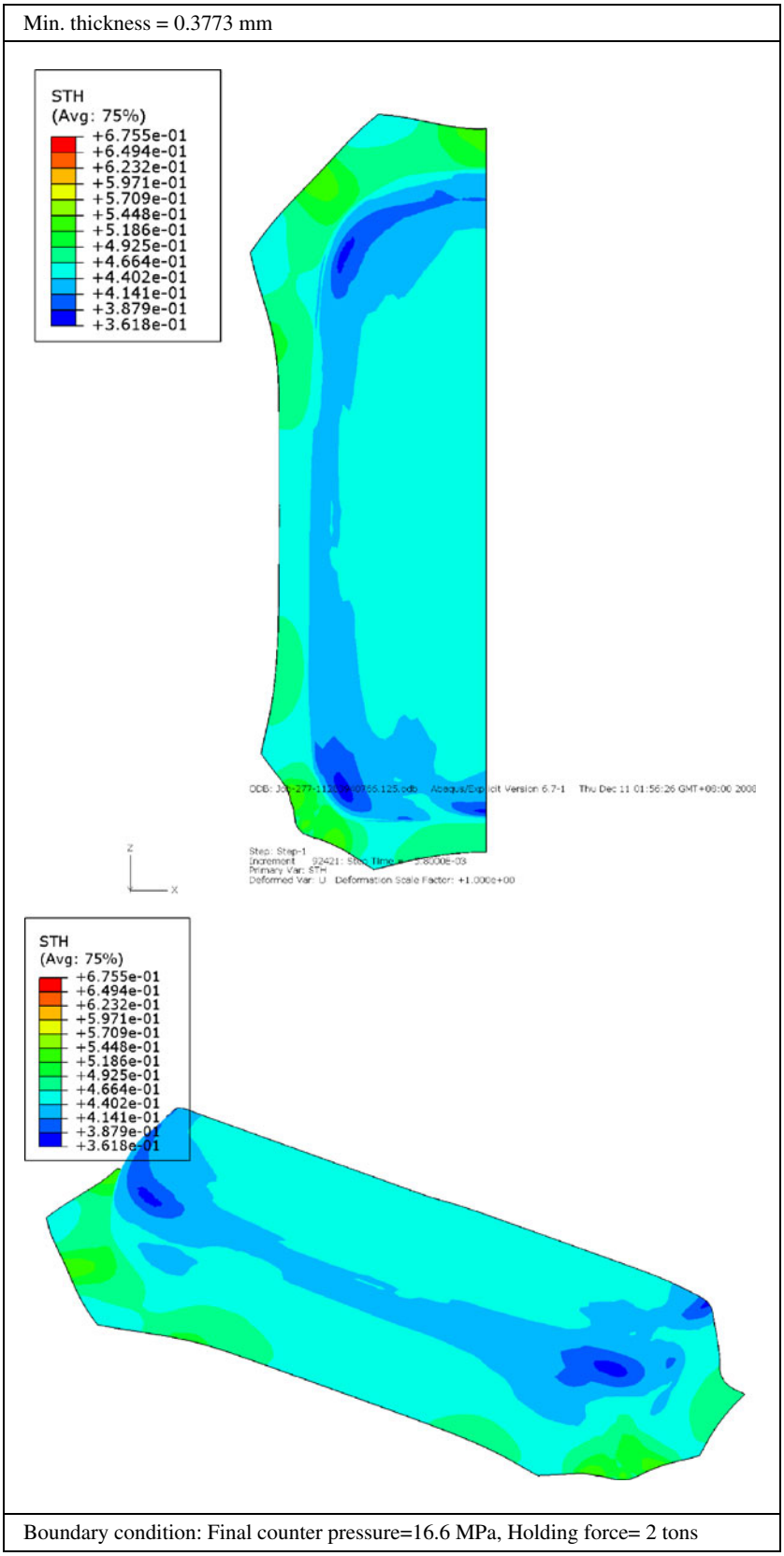


**Fig. 29** The thickness distribution of the blank (chamfer width=20 mm, SUS 304)

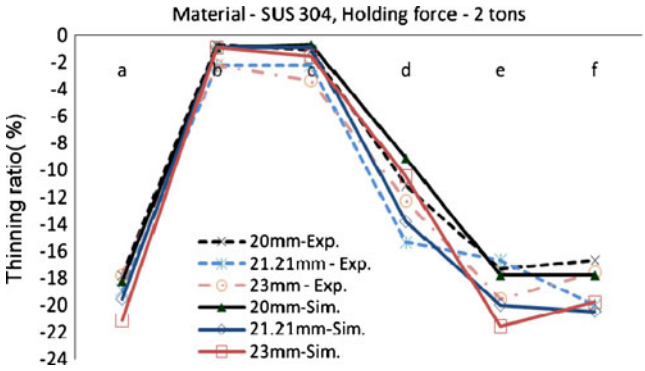


**Fig. 30** Results of thinning ratio distributions by simulation and experiment (different chamfer widths, SUS 304)

## 5 Analysis of the application of SHF on housing II

In this section, housing II was deformed with SHF, and significant process parameters, such as the blank dimension (different chamfer widths, lengths, and widths of the blank) and the holding force were again analyzed and verified by experiment and FE simulation. In some cases, stainless steel sheet (SUS 304) was also adopted as the working material to be compared with Ti/Al clad metal. Table 3 shows the combinations of process parameters for housing II. Figure 25 shows the locations of the measured points on housing II. Figure 26 shows the representation of the blank dimension.

### 5.1 Influence of blank dimensions (SUS 304)

In this section, three different blank dimensions were simulated for housing II. In the simulation, the Coulomb coefficient of friction was set to 0.05 (blank–die) and 0.1 (punch–blank and holder–blank) for contact surfaces with and without lubrication. Figures 27, 28, and 29 show the thickness distributions with different chamfer widths. Figure 30 shows the numerical and experimental comparison of thinning ratio distributions of the blank.

The simulation results shown in Figs. 27, 28, and 29 reveal that the minimum final thickness for a chamfer of 20 mm was higher than that for 23 and 21.21 mm, and an insignificant wrinkling occurs on the side of the blanks. As shown in Figs. 30, 31, the thinning distribution for a chamfer of 20 mm (black line) was much stable from both simulation and experiment results.

### 5.2 Comparisons of formability of SUS 304 and Ti/Al clad metal

In this section, Ti/Al clad metal sheets and SUS 304 sheets were simulated with different holding forces and their formability were compared. In simulation, the Coulomb coefficient of friction was set to 0.05 (blank–die) and 0.1 (punch–blank and holder–blank) for contact surfaces with and without lubrication. Figures 32, 33, 34, and 35 show the thickness distributions for different holding forces. Figure 36 shows the thinning ratio distribution of the blank with different parameter combinations.

These simulation results show that the formability of the blank was best when the blank dimensions were: length, 114 mm; width, 74 mm; and chamfer width, 20 mm.

Comparison of the thinning ratios for Ti/Al clad metal sheet with those of SUS 304 sheet in specific cases (holding forces of 0.7 and 1 t and chamfer width of 20 mm) showed that the thinning ratio of clad metal sheet was thinner (−26%) than that of the SUS 304 sheet cases. Figure 37 shows that the failure of blank occurs at point a.

Overall, the tendency of the thickness distributions of the Ti/Al clad metal and SUS 304 sheet was similar in FE simulation. Figure 38 shows a product of Ti/Al clad metal sheet without failure (holding force, 0.7 t; chamfer width, 20 mm), which proves that a Ti/Al clad metal sheet with low formability can be successfully manufactured for 3C product applications by choosing suitable process parameters in SHF.

Figure 39 shows comparisons of the thinning ratio distributions from experiments and FE simulation. The tendencies of thinning ratios were in good agreement and the only difference was at point e, where the thickness was measured according to a single element in numerical post-processing. If an average thickness was measured from several elements, the result was close to that of the experimental data.

The simulation results indicate that the holding force is a significant parameter for metal flow. In housing I, the holding force of 2–3 t provides better formability; in housing II, the optimum holding force is 0.7 t. For counter pressure history, a higher final pressure can be helpful for drawing in the blank by supplying the blank with a more normal force. Suitable blank dimensions can be helpful for decreasing thinning. For the application of housing II, the chamfer width of 20 mm (114×74 mm) should be used for

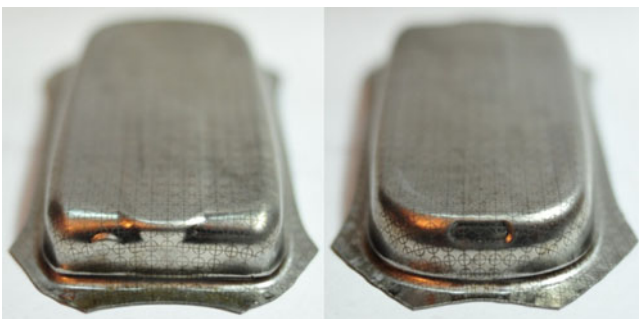

**Fig. 31** Deformation of SUS 304 without fracture (holding force, 2 t; chamfer width, 20 mm)

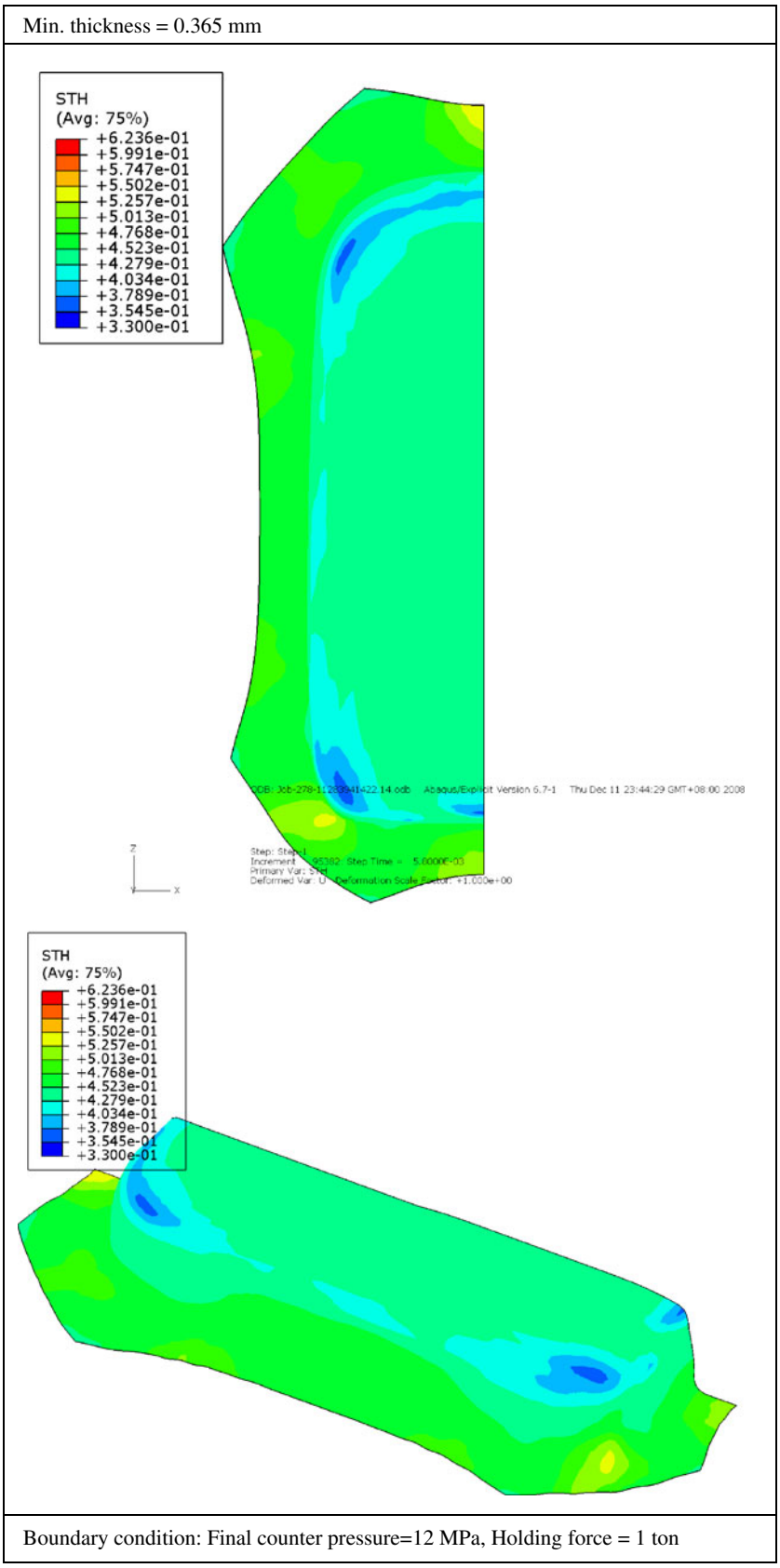


**Fig. 32** The thickness distribution of the blank (chamfer width=21.21 mm, SUS 304 sheet)

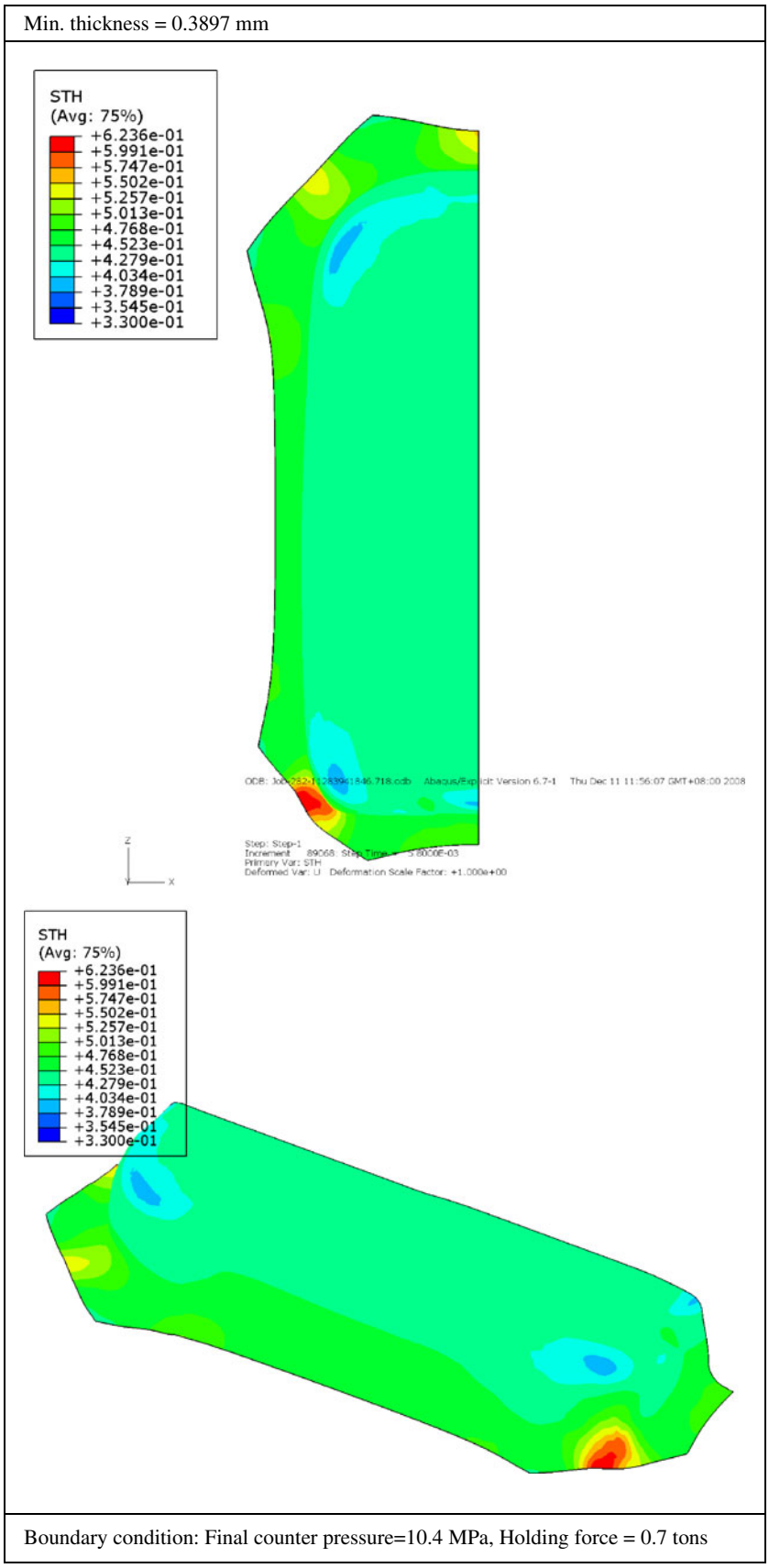


**Fig. 33** The thickness distribution of the blank (chamfer width=20 mm, SUS 304 sheet)

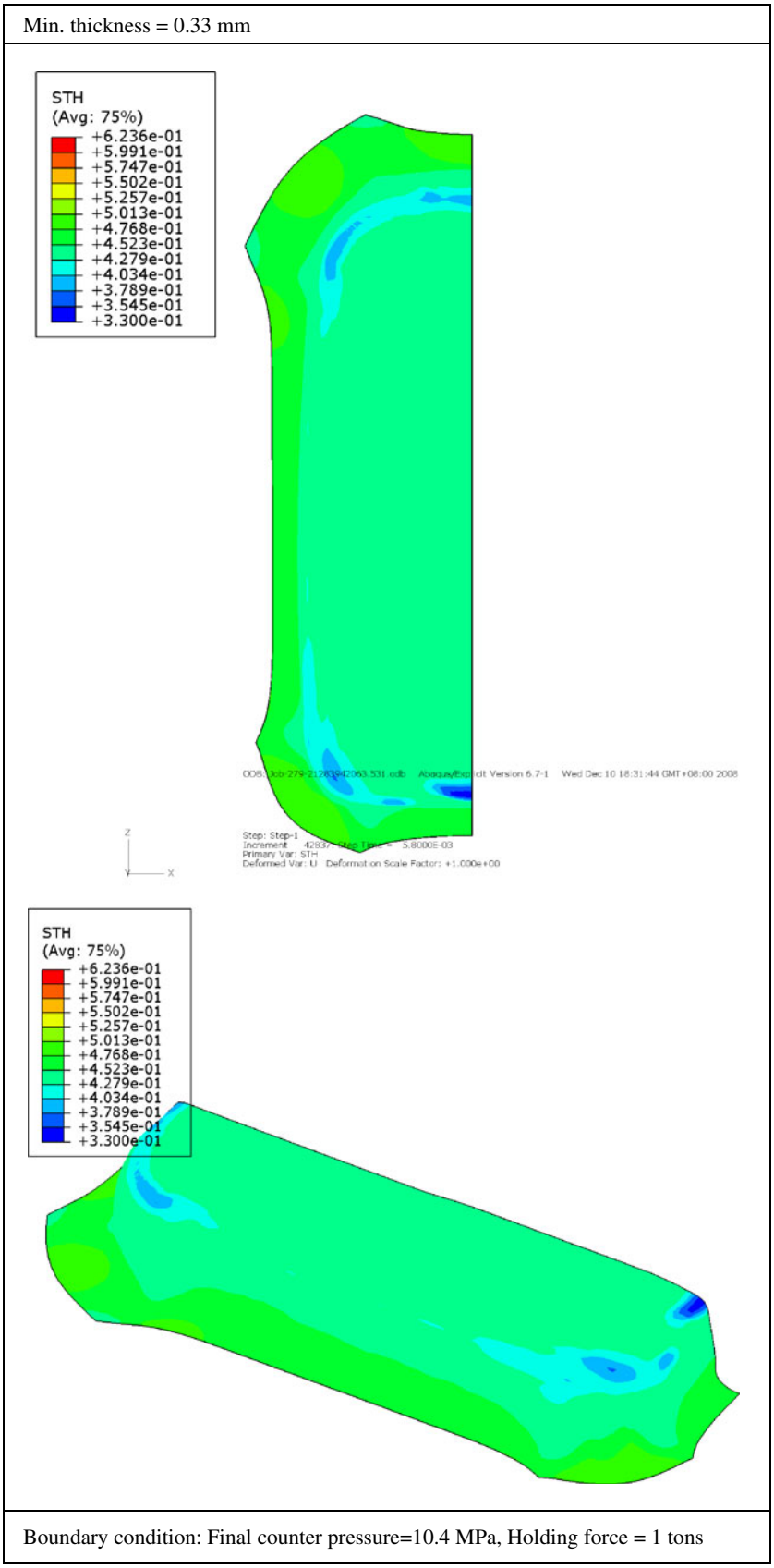


**Fig. 34** The thickness distribution of the blank (chamfer width=20 mm, Ti/Al clad metal)

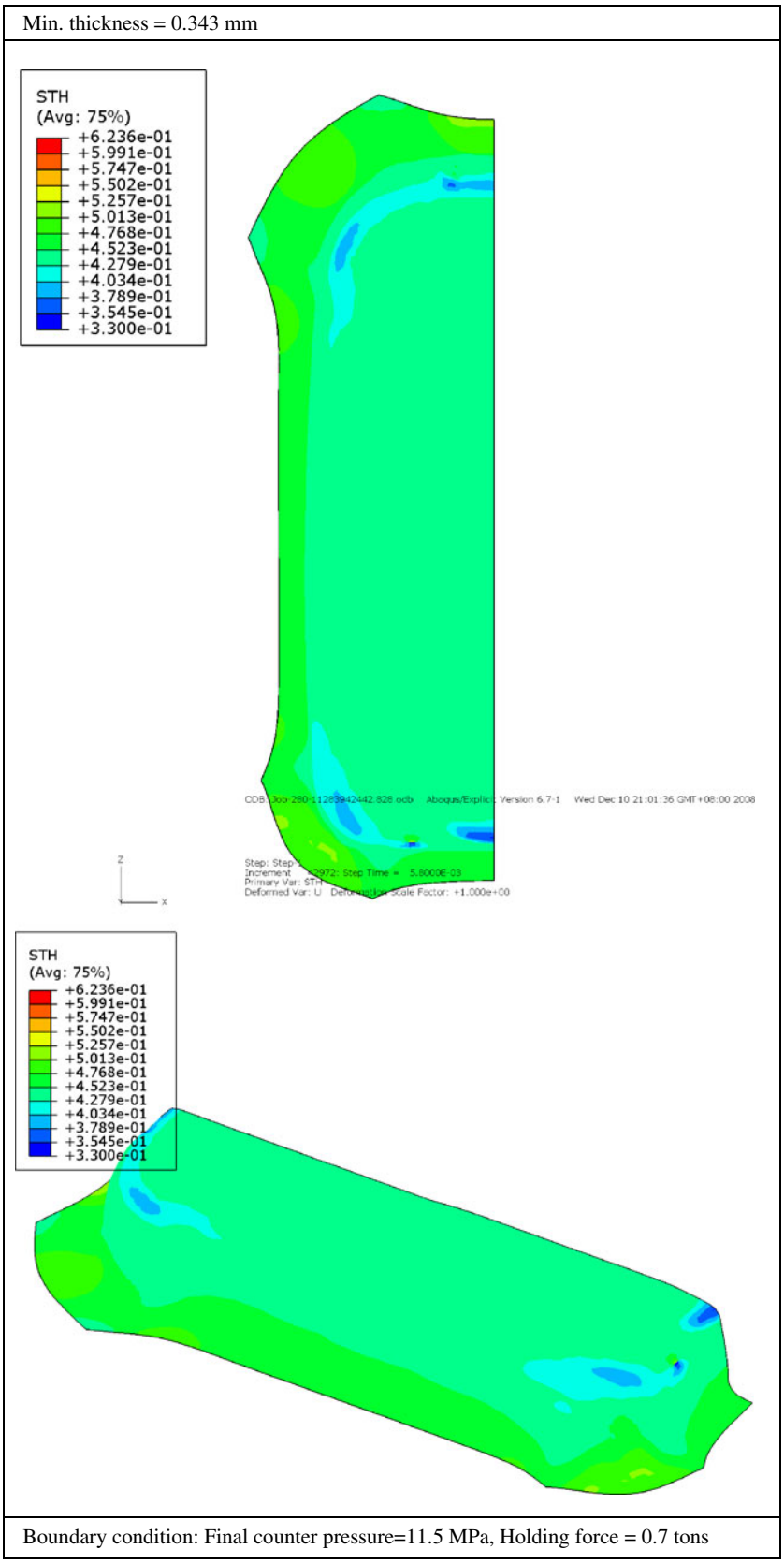


**Fig. 35** The thickness distribution of the blank (chamfer width=20 mm, Ti/Al clad metal)

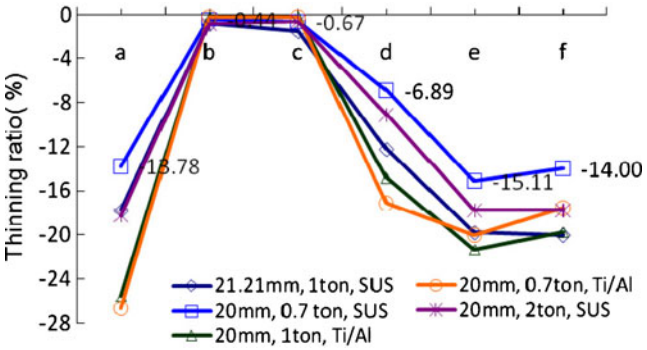


**Fig. 36** Comparison of thinning ratio distribution with different holding forces and chamfer widths for Ti/Al clad metal and SUS 304


**Fig. 37** Failure of the Ti Al clad metal housing occurs at point a (holding force, 1 t; chamfer width, 20 mm)

**Fig. 38** Ti/Al clad metal housing without failure (holding force, 0.7 t; chamfer width, 20 mm)

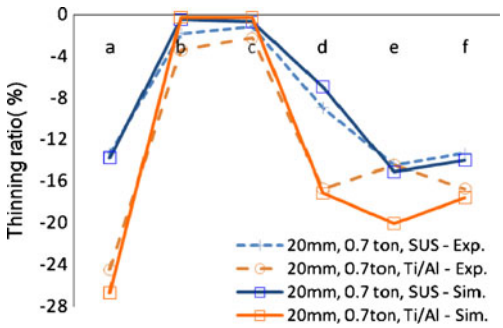


**Fig. 39** Comparison of thinning ratio distributions from experiments and FE simulation

the initial blank shape. Compared to SUS 304 sheet, the Ti/Al clad metal sheet with low formability can achieve the same product quality if suitable parameters are chosen in SHF.

## 6 Conclusions

This research has discussed several significant process parameters for the formability of Ti/Al clad metal sheet during SHF. Some tasks accomplished were: (a) the material property of a Ti/Al clad metal sheet (0.45 mm thick) was obtained; (b) the SHF FE model was validated; and (c) the results of simulation and experiments for the applications of Ti/Al clad metal sheets during SHF were compared.

In SHF simulation, a virtual film technique was proposed and successfully simulated the hydraulic loading for clad metal sheets during SHF.

From the simulation results, sufficient friction force and high final counter pressure has been found to be helpful for drawing in the blank. Suitable blank dimensions (chamfer width) can also be helpful for decreasing the thinning effect. By choosing suitable parameters, the Ti/Al clad metal sheet with low formability can achieve the same product quality as that provided by SUS 304 sheet.

**Acknowledgments** The authors would like to thank Metal Industries Research & Development Centre (MIRDC) for its support of this research project and Mr. Lee and Dr. Chiang for their assistance in fabricating the clad metal sheet. Simulations in this research were partly performed at the National Center for High-Performance Computing.

## References

1. Özdemir N, Bilgin B (2009) Interfacial properties of diffusion bonded Ti-6Al-4V to AISI 304 stainless steel by inserting a Cu interlayer. Int J Adv Manuf Technol 35:814–820. doi:10.1007/s00170-008-1493-6
2. Masahashi N, Komatsu K, Kimura G, Watanabe S, Hanada S (2006) Fabrication of iron aluminum alloy/steel laminate by clad rolling. Metall Mater Trans A 37A:1665–1673. doi:10.1007/s11661-006-0108-9
3. Kim JK, Huh MY, Lee JC (2004) Evolution of strain states and textures during roll-cladding in STS/Al/STS sheets. J Mater Sci 39:5371–5374. doi:10.1023/B:JMSC.0000039247.10346.5d
4. Kang HG, Kim JK, Huh MY, Engler O (2007) A combined texture and FEM study of strain states during roll-cladding of five-ply stainless steel/aluminum composites. Mat Sci Eng A 452–453:347–358. doi:10.1016/j.msea.2006.10.130
5. Schmoeckel D, Hielscher C, Huber R (1999) Metal forming of tubes and sheets with liquid and other flexible media. Ann CIRP 48(2):1–20
6. Schnupp K, Kerschner M (2003) Presses for hydromechanical drawing of panels for automobiles. Hydroforming of tubes, extrusions and sheet metals 3:409–421
7. Bruni C, Celeghini M, Geiger M, Gabrielli F (2007) A study of techniques in the evaluation of springback and residual stress in hydroforming. Int J Adv Manuf Technol 33:929–939

8. Kim J, Kang YH, Choi HH, Hwang SM, Kang BS (2002) Comparison of implicit and explicit finite element methods for the hydroforming process of an automobile lower arm. Int J Adv Manuf Technol 20:407–413
9. Lang L, Li T, An D, Chi C, Nielsen KB, Danckert J (2009) Investigation into hydromechanical deep drawing of aluminum alloy—complicated components in aircraft manufacturing. Mat Sci Eng A 499:320–324
10. Kim TJ, Yang DY, Han SS (2004) Numerical modeling of the multi-stage sheet pair hydroforming process. J Mater Proc Technol 151:48–53
11. Chen W, Liu ZJ, Hou B, Du RX (2007) Study on multi-stage sheet metal forming for automobile structure-pieces. J Mater Proc Technol 187–188:113–117
12. Palumbo G, Zhang SH, Tricarico L, Xu C, Zhou LX (2006) Numerical/experimental investigations for enhancing the sheet hydroforming process. Int J Mach Tool Manuf 46:1212–1221
13. Zhang SH, Zhou LX, Wang ZT, Xu Y (2003) Technology of sheet hydroforming with a moveable female die. Int J Mach Tool Manuf 43:781–785
14. Thiruvarudchelvan S, Tan MJ (2007) Fluid-pressure-assisted deep drawing. J Mater Proc Technol 192–193:8–12
15. Danckert J, Nielsen KB (2000) Hydromechanical deep drawing with uniform pressure on the flange. CIRP Ann—Manuf Technol 49–1:217–220
16. Kleiner M, Krux R, Homberg W (2004) Analysis of residual stresses in high-pressure sheet metal forming. CIRP Ann—Manuf Technol 53–1:211–214
17. Tseng HC, Hung C, Huang CC (2009) An analysis on formability of aluminum/copper clad metal with different thickness by finite element method and experiment. Int J Adv Manuf Technol 49:1029–1036. doi:10.1007/s00170-009-2446-4
18. Groche P, Metz C (2005) Hydroforming of unwelded metal sheets using active-elastic tools. J Mater Proc Technol 168:195–201